Available online at www.sciencedirect.com
ScienceDirect
Journal of Power Sources 178 (2008) 476–482
JOURNAL OF POWER SOURCES
www.elsevier.com/locate/jpowsour

In situ X-ray absorption spectroscopic studies of anodically deposited binary Mn–Fe mixed oxides with relevance to pseudocapacitance

Ming-Tsung Lee [a], Jeng-Kuei Chang [a,*], Wen-Ta Tsai [a], Chung-Kwei Lin [b]

[a] *Department of Materials Science and Engineering, National Cheng Kung University, 1 University Road, Tainan 701, Taiwan*
[b] *Department of Materials Science, Feng Chia University, Taichang, Taiwan*

Received 16 October 2007; received in revised form 7 December 2007; accepted 11 December 2007
Available online 23 December 2007

Abstract

Binary Mn–Fe oxides with different Mn/Fe content ratios were prepared by anodic deposition. The deposited oxides were studied by in situ X-ray absorption spectroscopy (XAS) in 2 M KCl solution during the charging–discharging process. The experimental results clearly confirmed that the oxidation states of both Mn and Fe changed back and forth with adjusting the applied potential, contributing to the pseudocapacitive characteristics of the binary oxides. It was also found that, within a potential range of 1 V, because of Fe oxide addition the variation in the Mn oxidation state was increased from 0.70 (+3.25 to +3.95 for plain Mn oxide) to 0.81 (+3.12 to +3.93 for Mn90Fe10 oxide or +3.10 to +3.91 for Mn75Fe25 oxide), while the Fe oxide itself demonstrated an oxidation state shift of only 0.55. Accordingly, the optimum pseudocapacitance of the binary Mn–Fe oxide could be only achieved when the amount of Fe oxide was properly controlled. The highest specific capacitance of 255 F g^{-1} was obtained with a Mn/Fe atomic ratio of 90/10, while plain Mn oxide revealed a capacitance of only 205 F g^{-1}.

Keywords: Mn–Fe oxide; Pseudocapacitance; Super capacitor; X-ray absorption spectroscopy; In situ spectroscopy

1. Introduction

Super capacitors are charge-storage devices that have a greater power density and longer cycle life than batteries do, and a higher energy density than that of conventional capacitors [1]. They have attracted a lot of attention in many fields, e.g. hybrid power sources, peak power sources, backup power storage, lightweight electronic fuses, and starting power of fuel cells [2–4]. The natural abundance and low-cost of Mn oxide, accompanied by its satisfactory pseudocapacitive performance in mild electrolytes and environmental compatibility, have made it one of the most promising electrode materials for super capacitors. The preparation methods of Mn oxides for capacitor applications include thermal decomposition [5], co-precipitation [6–8], sol–gel processes [9–12], physical vapor deposition [13,14], hydrothermal synthesis [15], and anodic deposition [16–18].

In order to further improve the pseudocapacitive properties of plain Mn oxide, the addition of other transition metal oxides has been attempted. Studies have found that the incorporation of Ni [8,19], Pb [8], Co [19,20], V [21], and Mo [22] oxides could enhance the specific capacitances of Mn-based oxides. Recently, crystalline $MnFe_2O_4$ with a spinel structure, which could exhibit pseudocapacitive behavior, was found to have wonderful cyclic stability. However, its specific capacitance was only around 100 F g^{-1} [23,24]. In contrast, our previous study [25] indicated that hydrous Mn–Fe mixed oxide, in which the Mn oxide was nanocrystalline and the Fe oxide seemed to be amorphous in nature, can be prepared by anodic deposition. An optimum specific capacitance of the binary oxide was over 200 F g^{-1}. However, the detailed mechanism that governs the charge-storage performance has not been clearly disclosed yet. Whether or not Fe oxide participates in the pseudocapacitive reaction and how it affects the electrochemical performance of the Mn oxide are worthy of further investigation.

The energy storage mechanism of electrodeposited plain Mn oxide has been examined using in situ X-ray absorption spectroscopy (XAS) [26–28]; the chemical state variation of the Mn oxide as a function of applied potential was explored. It has been confirmed that the pseudocapacitance of the Mn

* Corresponding author. Tel.: +886 6 2757575x62942; fax: +886 6 2754395.
E-mail address: catalyst@mail.mse.ncku.edu.tw (J.-K. Chang).

0378-7753/$ – see front matter © 2007 Elsevier B.V. All rights reserved.
doi:10.1016/j.jpowsour.2007.12.032

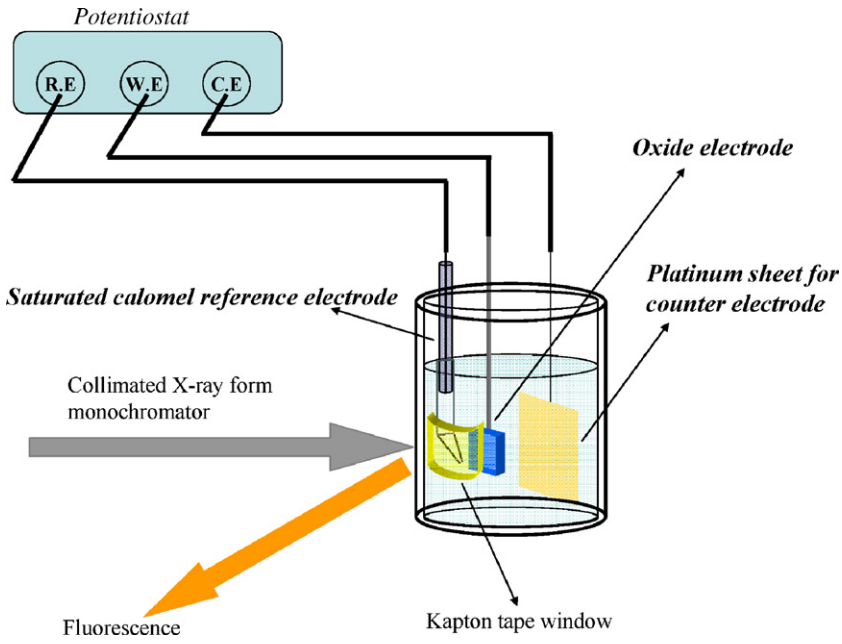

Fig. 1. A schematic of the spectroelectrochemical cell used for the in situ XAS study.

oxide can be ascribed to the continuous and reversible redox reaction between its trivalent and tetravalent forms. However, the binary Mn–Fe mixed oxide prepared by anodic deposition has never been investigated using in situ XAS. In this study, Mn and Fe–K edge XAS spectra of oxides with different Mn/Fe content ratios are studied during the electrode charging–discharging process. The relationship between the chemical composition and the pseudocapacitive performance of the binary oxide is discussed according to the in situ XAS data.

2. Experimental

Binary Mn–Fe mixed oxides were electroplated onto 1 cm × 1 cm graphite substrates by anodic deposition at 25 °C. The substrates were first polished with SiC paper of 800 grit, degreased with acetone, then etched in 0.2 M H_2SO_4, and finally washed with pure water in an ultrasonic bath. During the electrodeposition, a three-electrode electrochemical system was employed; the cell and instrument configurations are described elsewhere [29,30]. The anodic deposition was performed under a constant potential of 0.8 V versus a saturated calomel electrode (SCE) to give a total passed charge of 1.5 C; the typical thickness of the deposited oxides was approximately 4 μm. The plating solutions were 0.25 M $Mn(CH_3COO)_2$ aqueous solutions with various amounts of $FeCl_3$ added (up to 0.15 M). Our previous study [25] reported that the chemical composition of the deposited binary Mn–Fe oxide can be controlled by simply adjusting the $Mn(CH_3COO)_2/FeCl_3$ concentration ratio in the plating solution. In this paper, binary oxide containing a Mn/Fe atomic ratio of X/Y ($X+Y=100$) is denoted as MnXFeY oxide for brevity. The mass of the deposited oxide was determined by measuring the weight difference of the graphite substrate before and after the electrodeposition.

The pseudocapacitive performance of the deposited oxides was evaluated using cyclic voltammetry (CV) in 2 M KCl aqueous solution at 25 °C. The test was performed in a three-electrode cell, in which the oxide electrode was assembled as the working electrode. In addition, a platinum sheet and a SCE were used as the counter electrode and the reference electrode, respectively. The measuring instrument was an EG&G 263 potentiostat. For the CV test, the electrode potential was swept at a rate of 5 mV s^{-1} within a range of 0–1 V (vs. SCE). For the specific capacitance evaluation, five samples were tested and the data shown in this paper was the average.

Two binary oxides with Mn/Fe atomic ratios of 90/10 and 75/25, namely Mn90Fe10 and Mn75Fe25 oxide electrodes, were studied using in situ XAS in fluorescence mode. Fig. 1 shows the configuration of the spectroelectrochemical cell used in this study. The cell, which is filled with 2 M KCl solution, has a window sealed by fluorescence-transparent Kapton tape. A series of XAS spectra were acquired at different applied potentials, starting from 0 to 1 V and then back to 0 V with an interval of either 0.1 or 0.2 V. A larger potential step size reflected a higher potential changing rate during the test. Before taking the Mn and Fe–K edge spectra at a given potential of interest (the total acquisition time was about 40 min), the electrode was kept at that applied potential for 15 min while the oxide approached a steady state. The XAS experiments were performed at beam line 17C of the National Synchrotron Radiation Research Center (NSRRC) in Hsinchu, Taiwan. The storage ring was operated with an electron energy of 1.5 GeV and a current between 100 and 200 mA. A Si(1 1 1) double crystal monochromator was employed for energy selection. The X-ray absorption energy was calibrated using the first inflection point of the Mn–K edge main absorption region of a metallic Mn foil (6539.0 eV), which was measured before each XAS scan. Moreover, in order to identify the chemical states of the deposited binary oxides at the various applied

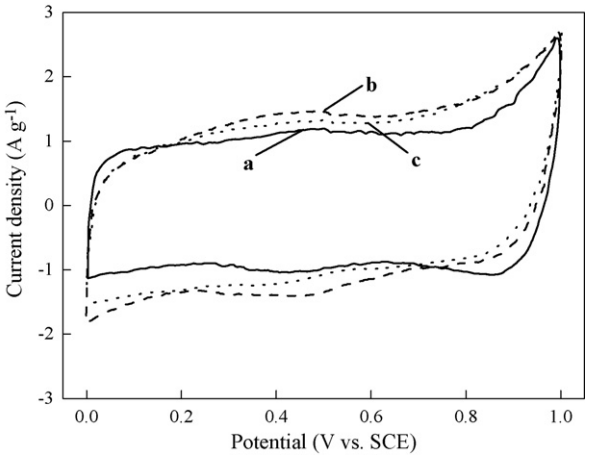

Fig. 2. Cyclic voltammograms of the three oxide electrodes measured in 2 M KCl solution at a potential scan rate of 5 mV s^{-1}. Curves a–c represent the plain Mn oxide, Mn90Fe10 oxide, and Mn75Fe25 oxide, respectively.

potentials, MnO, Mn_2O_3, MnO_2, Fe, FeO, and Fe_2O_3 standard samples were used as the references in XAS analyses.

3. Results and discussion

Electrochemical behavior of the deposited oxides was evaluated using CV in 2 M KCl solution with a potential scan rate of 5 mV s^{-1}. Fig. 2 shows the voltammograms of plain Mn oxide (curve a), Mn90Fe10 oxide (curve b), and Mn75Fe25 oxide (curve c) electrodes, respectively. The rectangular shapes and mirror-image characteristics of the three CV curves reveal the ideal pseudocapacitive behavior of all the electrodes, indicating that the deposited binary Mn–Fe oxides are promising electrode materials for use in super capacitors. In this figure, although the shapes of three CV curves are similar, the Mn90Fe10 oxide has the largest enclosed area, reflecting its superior charge-storage performance. To quantitatively evaluate the pseudocapacitance of the oxides, the specific voltammetric charge (based on oxide weight) of the three CV curves was integrated over the potential window of 0–1 V. The specific capacitance (C) of the oxides can be calculated by the following equation:

$$C = \frac{\text{specific voltammetric charge}}{\text{potential range}} \quad (1)$$

Fig. 3 shows the variation in specific capacitance of the prepared electrodes versus the Fe content in the binary oxides. The data indicates that the specific capacitance remarkably increases from 205 F g^{-1} for plain Mn oxide to 255 F g^{-1} for Mn90Fe10 oxide. However, further increasing the Fe content in the binary oxide causes the reverse effect; the specific capacitance of Mn65Fe35 oxide is only 190 F g^{-1}, which is even worse than that of plain Mn oxide. The experimental results, shown in Fig. 3, clearly show that the amount of Fe oxide added significantly affects the overall capacitance of the deposited binary Mn–Fe oxide. However, the detailed electrochemical mechanism that operates the pseudocapacitive performance of the oxide electrode has to be further investigated.

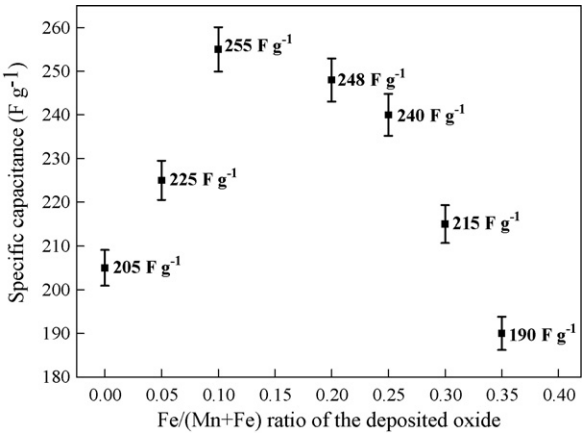

Fig. 3. The relationship between the specific capacitance and the chemical composition of the deposited binary Mn–Fe oxides.

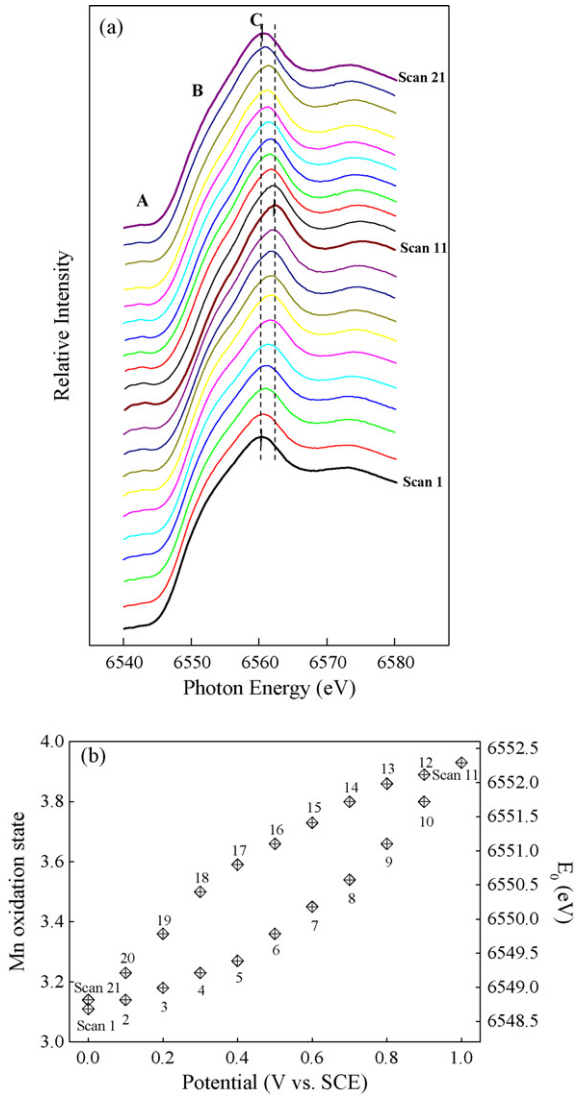

Fig. 4. (a) Twenty-one serial in situ Mn–K edge XAS spectra of the Mn90Fe10 oxide measured at various applied potentials. (b) The dependence of the Mn oxidation state with respect to the applied potential, obtained from (a).

In situ XAS measurements of the binary Mn–Fe oxides are performed in this study. Comparing the data to that obtained from plain Mn oxide (using a similar analytical method) as reported in our previous paper [27], the role of the incorporated Fe oxide can be verified. Fig. 4(a) shows the 21 serial Mn–K edge XAS spectra of the Mn90Fe10 oxide measured for a sequence of applied potentials, starting from 0 to 1 V and then back to 0 V with an interval of 0.1 V. As demonstrated, each spectrum can be divided into a pre-edge region (A), a main edge region (B), and a peak region (C), followed by an extended X-ray absorption fine structure (EXAFS) oscillation. The spectra, shown in Fig. 4(a), do not exhibit much difference in the shape, revealing a similarity in structural characteristics of the oxide under various applied potentials. This feature could explain the great cyclic stability of the oxide electrode during the charging–discharging process [25]. However, an energy shift of the adsorption peak, toward higher energy with increasing applied potential (scans 1–11) and then back toward lower energy as the potential was decreased (scans 11–21), can be clearly recognized in this figure. According to the literature [31,32], the valent state of Mn could be identified by the absorption threshold energy, E_0, which was obtained from the first inflection point on the main absorption edge. This so-called chemical shift is related to the increase in binding energy of the core-level electron with increasing the oxidation state, which is in turn caused by the reduced screening of the core-level by valence electrons [31]. Three reference samples of MnO(II), Mn_2O_3(III), and MnO_2(IV) were also analyzed in the XAS study; their E_0 values were found to be 6544.7, 6548.2, and 6552.6 eV, respectively. The results confirmed that the E_0 increased with increasing the Mn oxidation state. The E_0 values of the serial XAS scans shown in Fig. 4(a) are summarized in Table 1; the corresponding Mn oxidation states calculated according to the proportional relationship are also listed in this table. Fig. 4(b) shows the continuous and reversible change of the Mn oxidation state with respect to the applied potential; the valence is balanced by insertion/extraction of H^+ or K^+ into/from the oxide lattice. At the applied potential of 0 V, the oxide reveals an E_0 value of 6548.7 eV, corresponding to an Mn oxidation state of +3.11. As the potential is increased to 1 V step by step, the Mn oxidation state progressively increases to +3.93. Then, the oxidation state of Mn is gradually reduced to +3.14 when the applied potential is moved back to 0 V. It has been reported [27] that for plain Mn oxide, within the same potential range, the oxidation state shifts from +3.23 to +3.95 and then back to +3.27. Our previous paper [25] indicated that the following interplay reaction between Mn and Fe ions could occur, resulting in a reduction in the Mn oxidation state of the as-deposited oxide.

$$Mn^{4+} + Fe^{2+} \rightarrow Mn^{3+} + Fe^{3+} \quad (2)$$

This study further confirms that Fe oxide addition can extend the lower limit of the Mn oxidation state during in situ XAS analyses. Therefore, the variation in the Mn oxidation state can be enlarged from 0.70 for plain Mn oxide to 0.81 for the binary

Table 1
The E_0 values of the Mn–K edge and the pre-edge positions of the Fe–K edge serial XAS spectra of the Mn90Fe10 oxide measured for a sequence of applied potentials

Sample	Applied potential (V)	Scan sequence	E_0 (eV)	Mn oxidation state	Pre-edge position (eV)	Fe oxidation state
	0	1	6548.7	3.11	7114.5	2.45
	0.1	2	6548.8	3.14	7114.5	2.45
	0.2	3	6549.0	3.18	7114.5	2.45
	0.3	4	6549.2	3.23	7114.5	2.45
	0.4	5	6549.4	3.27	7114.6	2.54
	0.5	6	6549.8	3.36	7114.7	2.64
	0.6	7	6550.2	3.45	7114.8	2.73
	0.7	8	6550.6	3.55	7114.9	2.82
	0.8	9	6551.1	3.66	7115.0	2.91
	0.9	10	6551.7	3.8	7115.1	3
Deposited Mn90Fe10 oxide	1.0	11	6552.3	3.93	7115.1	3
	0.9	12	6552.1	3.89	7115.1	3
	0.8	13	6552.0	3.86	7115.1	3
	0.7	14	6551.7	3.80	7115.0	2.91
	0.6	15	6551.4	3.73	7114.9	2.82
	0.5	16	6551.1	3.66	7114.8	2.73
	0.4	17	6550.8	3.59	7114.7	2.64
	0.3	18	6550.4	3.50	7114.6	2.54
	0.2	19	6549.8	3.36	7114.5	2.45
	0.1	20	6549.2	3.23	7114.5	2.45
	0	21	6548.8	3.14	7114.5	2.45
MnO			6544.7	2		
Mn_2O_3			6548.2	3		
MnO_2			6552.6	4		
Fe					7112.0	0
FeO					7114.0	2
Fe_2O_3					7115.1	3

The corresponding Mn and Fe oxidation states calculated according to the reference samples are also listed.

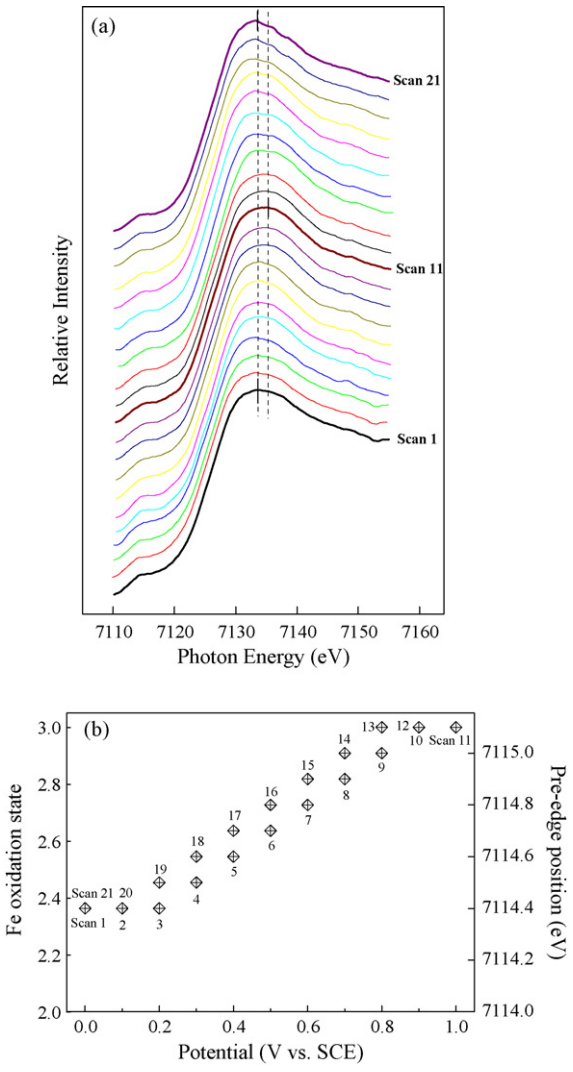

Fig. 5. (a) Twenty-one serial in situ Fe–K edge XAS spectra of the Mn90Fe10 oxide measured at various applied potentials. (b) The dependence of the Fe oxidation state with respect to the applied potential, obtained from (a).

Mn–Fe oxide within a potential range of 1 V. Moreover, Fig. 4(b) also reveals a hysteresis loop, presenting a delay of the oxidation state adjustment with respect to the applied potential; a detailed discussion is given in the literature [27]. This phenomenon is ascribed to the poor electronic and ionic conductivity of the Mn oxide [9,22,33,34].

Fig. 5(a) shows the serial Fe–K edge XAS spectra of the Mn90Fe10 oxide measured at various applied potentials. As illustrated, a chemical shift, in a similar manner to that observed in Fig. 4(a), is also recognized. It has been reported in the literature [32,35] that the oxidation state of Fe can be determined by the XAS pre-edge peak position. Three reference samples of Fe(0), FeO(II), and Fe_2O_3(III) were thus analyzed in this study; an approximately linear relationship between the Fe oxidation state and the pre-edge peak position was clearly recognized, as shown in Table 1. This table also lists the calculated Fe oxidation states which are obtained from the serial XAS spectra shown in Fig. 5(a). Fig. 5(b) demonstrates the variation of the Fe oxidation state of the Mn90Fe10 oxide with respect to the applied potential. Two facts should be emphasized according to the analytical data: (i) the Fe oxide in the electrode participates in the electrochemical redox reaction; the pseudocapacitive behavior of the binary oxide electrodes, as characterized by the CV curves in Fig. 2, can be attributed to the continuous and reversible changes in the oxidation states of both Mn and Fe cations during the charging–discharging process; (ii) in the potential range of 0–1 V, the change in the Fe oxidation state is only 0.55, varying from +2.45 to +3. This value (0.55) is much smaller than the change in the Mn oxidation state (0.81) within the same potential range. Of note, since the fluorescence mode was adopted in the XAS study, the analytical signal was collected from a sub-micrometer depth beneath the sample surface [36,37]. Accordingly, the experimental results clearly indicate that the faradic redox reaction is not restricted to being only near the surface, but is also involved within the bulk of the oxide.

The in situ XAS analyses were also done for the Mn75Fe25 oxide with different potential step sizes. Since the XAS acquisition time under each applied potential was identical, a larger step size reflected a higher potential changing rate. Fig. 6(A) shows the Mn oxidation state variation as a function of the applied potential, obtained from the in situ Mn–K edge XAS spectra, but with different potential step sizes of 0.1 V (for the curve a) and 0.2 V (for the curve b), respectively. It is noted that, with the step size of 0.1 V, the oxidation state of Mn increases from +3.09 (at 0 V) to +3.91 (at 1 V) and then back to +3.11 (at 0 V). The change in the Mn oxidation state within the potential range is about 0.81, which is similar to that of the Mn90Fe10 oxide.

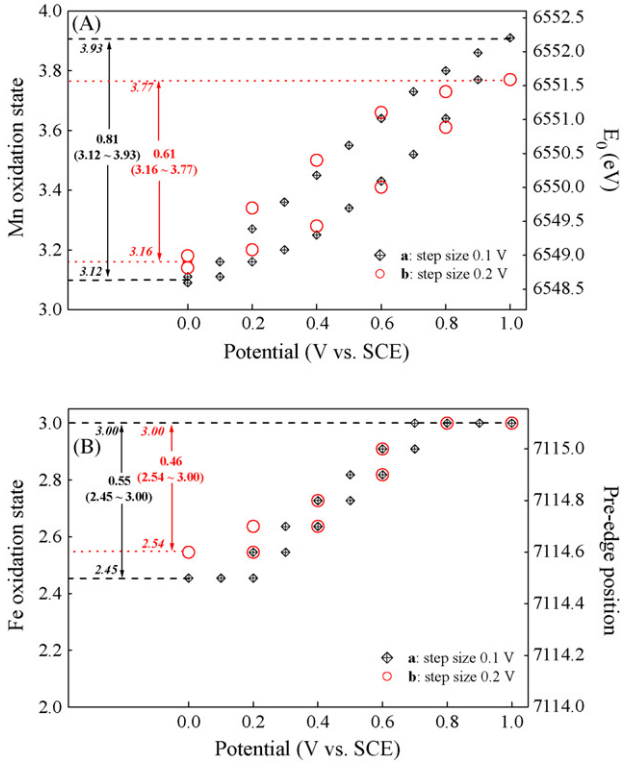

Fig. 6. The variations in the (A) Mn and (B) Fe oxidation states during the in situ XAS studies performed at the potential step sizes of 0.1 V (curve a) and 0.2 V (curve b). All the data was collected from the Mn75Fe25 oxide.

Table 2
The specific capacitances (from the CV tests) of the three deposited oxides and the Mn and Fe oxidation state variations during the in situ XAS measurements

Sample	Specific capacitance ($F\,g^{-1}$) (evaluated at a CV scan rate of $5\,mV\,s^{-1}$)	Mn oxidation state variation (from in situ XAS)	Fe oxidation state variation (from in situ XAS)	Average change in oxidation state per cation
Mn oxide	205	3.25–3.95	–	0.70
Mn90Fe10 oxide	255	3.12–3.93	2.45–3.00	0.78[a]
Mn75Fe25 oxide	240	3.10–3.91	2.45–3.00	0.75[b]

[a] $[(3.93-3.12)\times 0.90]+[(3.00-2.45)\times 0.10]=0.78$.
[b] $[(3.91-3.10)\times 0.75]+[(3.00-2.45)\times 0.25]=0.75$.

The analytical data again supports that the degree of change of the Mn oxidation state during the charging–discharging process is increased by the incorporated Fe oxide; however, this increase levels off after a large amount of Fe oxide has been added. This figure also shows that the Mn oxidation state variation decreases notably to 0.61 when a larger potential step size of 0.2 V is adopted. This result further reveals the poor reaction kinetics of the Mn oxide. On the other hand, Fig. 6(B) shows the variation in the Fe oxidation state versus applied potential for the Mn75Fe25 oxide with different potential step sizes. The changes of the Fe oxidation state within the potential range of 0–1 V are 0.55 and 0.46 measured at the potential step sizes of 0.1 V (curve a) and 0.2 V (curve b), respectively. Unlike the considerable difference in the degree of change of the Mn oxidation state ($0.81-0.61=0.20$) when the potential step size increased from 0.1 to 0.2 V, that of Fe is much smaller ($0.55-0.46=0.09$). The analytical result implies that the Fe oxide has better kinetic performance compared to the Mn oxide. This claim is further supported by the fact that the hysteresis loop of Fe shown in Fig. 6(B) is less pronounced than that of Mn shown in Fig. 6(A).

According to the above in situ XAS data, the variation in specific capacitance of the binary Mn–Fe oxides as a function of chemical composition (as demonstrated in Fig. 3) can be explained. It has been found that the degree of change of the Mn oxidation state is increased from 0.70 to 0.81 by the Fe oxide incorporation (measured at a XAS potential step size of 0.1 V); however, adding even more Fe oxide does not further improve this value. The Fe oxide itself has a much smaller change in the oxidation state (0.55) compared to the Mn oxide (0.81) within the same potential range. Taking both factors into account, the optimum specific capacitance of the binary Mn–Fe oxide with a proper Mn/Fe content ratio is expected. Table 2 compares the specific capacitances of the three oxides with different Mn/Fe ratios with the average changes in oxidation state per cation (includes Mn and Fe) for the various samples; it is noted that the larger the change in oxidation state per cation is, the higher the specific capacitance that can be obtained. This consistency between the oxidation state change and the specific capacitance has again confirmed that the pseudocapacitive performance of the binary electrodes is governed by the faradic redox reactions of both the Mn and Fe oxides. However, according to the shift in the oxidation state within a potential range of 1 V, the theoretical pseudocapacitance of the oxides should be around $800\,F\,g^{-1}$, which is much higher than the practical capacitances shown in Table 2. The difference can be mainly ascribed to the poor conductivity of the oxide which kinetically limits it from delivering the ideal pseudocapacitance [27]. The in situ XAS study was performed under a potentiostatic condition (took about 1 h for the XAS scan at each potential step), which allowed a much longer reaction period than that during the CV test, so a larger change in the oxidation state analyzed by this method can be expected. This contention is well supported by the fact that using a larger potential step size (reflecting a higher potential changing rate) in the in situ XAS study can lead to a smaller change in the oxidation state, as demonstrated in Fig. 6. It is also noticed in Table 2 that although the average change in oxidation state per cation of the Mn90Fe10 oxide (0.78) is only 11% larger than that (0.70) of the plain Mn oxide, the former electrode exhibits a 24% higher specific capacitance than the latter, as evaluated using the CV tests. This result could be attributed to the superior kinetic performance of the binary Mn–Fe oxide compared with that of the plain Mn oxide.

4. Conclusions

Binary Mn–Fe oxides prepared by anodic deposition were studied using in situ XAS. The results confirm that the pseudocapacitive behavior of the binary oxides is associated with the continuous and reversible variations in the oxidation states of both the Mn and Fe cations with respect to the applied potential. For the Mn90Fe10 oxide, although the incorporated Fe oxide itself exhibits a shift in the oxidation state of only 0.55 within the potential range of 0–1 V, it evidently increases the change of the Mn oxidation state from 0.70 to 0.81. As a result, the specific capacitance of the Mn90Fe10 oxide ($255\,F\,g^{-1}$) is higher than that of the plain Mn oxide ($205\,F\,g^{-1}$). However, the analytical results indicate that further increasing the Fe oxide amount (i.e. the Mn75Fe25 oxide) does not increase the change of the Mn oxidation state. Moreover, taking the small shift in the Fe oxidation state into account, a high Fe/Mn ratio of the oxide causes a reduction in the specific capacitance. It is also found that the deposited Fe oxide seems to have superior kinetic performance of the pseudocapacitive redox reaction, as compared to the Mn oxide.

Acknowledgements

The authors would like to thank the National Science Council of the Republic of China for financially supporting this research (under Contract No. NSC 95–2221–E–006–192). The help from Dr. Jyh-Fu Lee and Mr. Cheng-An Hsieh for the in situ XAS experiment performed at NSRRC is greatly appreciated.

References

[1] R. Kötz, M. Carlen, Electrochim. Acta 45 (2000) 2483–2498.
[2] B.E. Conway, J. Electrochem. Soc. 138 (1991) 1539–1548.
[3] M. Ishikawa, M. Morita, M. Ihara, Y. Matsuda, J. Electrochem. Soc. 141 (1994) 1730–1734.
[4] J.P. Zheng, J. Huang, T.R. Jow, J. Electrochem. Soc. 144 (1997) 2026–2031.
[5] H.Y. Lee, V. Manivannan, J.B. Goodenough, C. R. Chim. 2 (1999) 565–577.
[6] H.Y. Lee, J.B. Goodenough, J. Solid State Chem. 144 (1999) 220–223.
[7] M. Toupin, T. Brousse, D. Bélanger, Chem. Mater. 14 (2002) 3946–3952.
[8] H. Kim, N. Branko Popov, J. Electrochem. Soc. 150 (2003) D56–D62.
[9] S.C. Pang, M.A. Anderson, T.W. Chapman, J. Electrochem. Soc. 147 (2000) 444–450.
[10] S.C. Pang, M.A. Anderson, J. Mater. Res. 15 (2000) 2096–2106.
[11] Y.U. Jeong, A. Manthiram, J. Electrochem. Soc. 149 (2002) A1419–A1422.
[12] R.N. Reddy, R.G. Reddy, J. Power Sources 124 (2003) 330–337.
[13] J.N. Broughton, M.J. Brett, Electrochem. Solid-State Lett. 5 (2002) A279–A282.
[14] B. Djurfors, J.N. Broughton, M.J. Brett, D.G. Ivey, J. Mater. Sci. 38 (2003) 4817–4830.
[15] V. Subramanian, H. Zhu, R. Vajtai, P.M. Ajayan, B. Wei, J. Phys. Chem. B 109 (2005) 20207–20214.
[16] C.C. Hu, T.W. Tsou, Electrochem. Commun. 4 (2002) 105–109.
[17] J.K. Chang, W.T. Tsai, J. Electrochem. Soc. 150 (2003) A1333–A1388.
[18] J.K. Chang, W.T. Tsai, J. Appl. Electrochem. 34 (2004) 953–961.
[19] K.R. Prasad, N. Miura, Electrochem. Commun. 6 (2004) 1004–1008.
[20] G.Y. Zhao, C.L. Xu, H.L. Li, J. Power Sources 163 (2007) 1132–1136.
[21] M. Nakayama, A. Tanaka, S. Konishi, K. Ogura, J. Mater. Res. 19 (2004) 1509–1515.
[22] M. Nakayama, A. Tanaka, Y. Sato, T. Tonosaki, K. Ogura, Langmuir 21 (2005) 5907–5913.
[23] S.L. Kuo, N.L. Wu, Electrochem. Solid-State Lett. 8 (2005) A495–A499.
[24] S.L. Kuo, J.F. Lee, N.L. Wu, J. Electrochem. Soc. 154 (2007) A34–A38.
[25] M.T. Lee, J.K. Chang, W.T. Tsai, J. Electrochem. Soc. 154 (2007) A875–A881.
[26] K.W. Nam, M.G. Kim, K.B. Kim, J. Phys. Chem. C 111 (2007) 749–758.
[27] J.K. Chang, M.T. Lee, W.T. Tsai, J. Power Sources 166 (2007) 590–594.
[28] S.L. Kuo, N.L. Wu, J. Electrochem. Soc. 153 (2006) A1317–A1324.
[29] J.K. Chang, Y.L. Chen, W.T. Tsai, J. Power Sources 135 (2004) 344–353.
[30] J.K. Chang, W.T. Tsai, J. Electrochem. Soc. 152 (2005) A2063–A2068.
[31] M. Belli, A. Scafati, A. Bianconi, S. Mobilio, L. Palladino, A. Reale, E. Burattini, Solid State Commun. 35 (1980) 355–361.
[32] P. Ghigna, G. Flor, G. Spinolo, J. Solid State Chem. 149 (2000) 252–255.
[33] H.Y. Lee, S.W. Kim, H.Y. Lee, Electrochem. Solid-State Lett. 4 (2001) A19–A22.
[34] J.K. Chang, C.T. Lin, W.T. Tsai, Electrochem. Commun. 6 (2004) 666–671.
[35] A. Deb, U. Bergmann, S.P. Cramer, E.J. Cairns, Electrochim. Acta 50 (2005) 5200–5207.
[36] J. Stöhr, NEXAFS Spectroscopy, Springer-Verlag, New York, 1992.
[37] H.B. Garg, E.A. Stern, D. Norman, X-ray Absorption in Bulk and Surfaces, World Scientific Publishing Co., Singapore, 1994.